DOI: 10.1002/chem.201000734

Excited-State Prototropic Equilibrium Dynamics of 6-Hydroxyquinoline Encapsulated in Microporous Catalytic Faujasite Zeolites

Sun-Young Park,[a] Hyunung Yu,[a, b] Jiho Park,[a, c] and Du-Jeon Jang*[a]

Abstract: The excited-state proton transfer and geminate recombination of 6-hydroxyquinoline (6HQ) encaged in catalytic Na^+-exchanged faujasite zeolites X (NaX) and Y (NaY) have been explored by measuring steady-state and picosecond time-resolved spectra. The pathways and rate constants of proton transfer of excited 6HQ are determined by the microscopic environment of zeolitic hosts surrounding the guest molecules. The excited-state proton transfer of a 6HQ molecule encapsulated in a zeolitic nanocavity is initiated by deprotonation of the enolic group to form an anionic intermediate and completed by subsequent protonation of the imino group to form a zwitterionic tautomer. Geminate recombination occurs to compete with proton transfer at each tautomerization step of excited-state 6HQ because of the confined environment of dehydrated zeolitic supercages. Consequently, excited-state equilibria among three prototropic species of 6HQ are established in microporous catalytic faujasite zeolites. Kinetic differences in NaX and NaY are attributed to dissimilarities in acidity/basicity.

Keywords: acid–base equilibria · geminate recombination · host–guest systems · proton transport · zeolites

Introduction

Zeolites, which are aluminosilicate materials with nanometer-sized void spaces in the form of cages or channels, have been the subject of growing interest because they can be widely used as solid catalysts in many technological and economical applications.[1–4] In particular, they are used as shape-selective catalysts in the production of biofuels as well as in petrochemical processes, such as cracking and reforming.[5–7] They can be also used as host systems for diverse organic molecules to control the photochemical behavior of the encaged guest molecules.[8] Host–guest systems are applicable in various fields, such as ion exchange, catalysis, sensing, and supramolecular organization.[9–14] These widespread applications of zeolites are mainly attributed to their catalytic activity,[15–19] which is mainly due to the presence of Brønsted acid/base sites. The acid/base sites of zeolites are capable of adsorbing guest molecules by strong hydrogen-bonding interactions and lead to protonation or deprotonation of the guest molecules. Accordingly, special attention has been paid to the structures of products generated through acid–base interactions between guest molecules and host zeolites, and various experimental methods have been employed to deduce whether the products have protonated or deprotonated structures.[19–24] However, to understand the roles of acid/base sites thoroughly in catalytic processes of zeolites, it is vital to investigate the elementary steps of interactions between guest molecules and catalytic sites (Brønsted acid/base sites) in the host zeolites.

Synthetic faujasites of X and Y types are among the most intensively used zeolites.[17–19] Both X and Y zeolites have a faujasite framework, with a cage 13 Å in diameter interconnected by four 8 Å windows (Figure 1). However, X and Y zeolites have different Si/Al ratios, and thus their internal spaces have dissimilar polarities. Acid/base properties of zeolites are known to be dependent on Si/Al ratios as well as on preparation methods such as dehydration.[25] The acidities of zeolites increase as Si/Al ratios increase, as protons replace metal cations, or as exchanged metal cations have

[a] S.-Y. Park, H. Yu, J. Park, D.-J. Jang
S.-Y. Park, Dr. H. Yu, Prof. Dr. J. Park, Prof. Dr. D.-J. Jang
School of Chemistry, Seoul National University
NS60, Seoul 151-742 (Korea)
Fax: (+82) 2-875-6624
E-mail: djjang@snu.ac.kr

[b] H. Yu
Korea Research Institute of Standards and Science
Daejeon 305-600 (Korea)

[c] J. Park
Department of Environmental Health
Korea National Open University
Seoul 110-791 (Korea)

Supporting information for this article is available on the WWW under http://dx.doi.org/10.1002/chem.201000734.

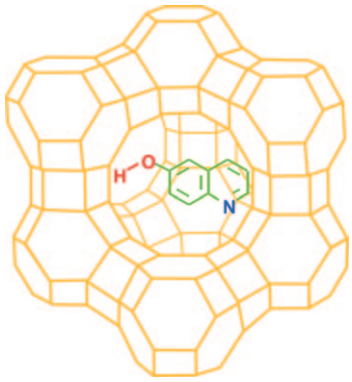

Figure 1. 6HQ encapsulated in a faujasite zeolitic nanocavity.

higher charge density.[26,27] Experimental studies have suggested that the number of protons located in a zeolitic supercage is 29 per unit cell and that the acidity of a proton-exchanged zeolite is as strong as that of a 70% aqueous solution of H_2SO_4.[28–31]

Proton-transfer reactions have been extensively investigated because they play important roles in a wide variety of chemical and biological processes.[25,32–49] Zeolites are fascinating media to study the proton-transfer dynamics of guest molecules without interference by solvent reorganization that occurs in solvents and makes it difficult to directly observe intrinsic proton transfer. Exploration of the proton-transfer dynamics of adsorbed molecules in zeolites helps to understand encapsulation effects of adsorbates confined in host materials as well as the catalytic activities of zeolites. Photoinitiated processes of guest chromophores encaged in host materials have been attracting considerable attention due to novel applications in diverse fields.[25,45–50] In particular, applications as artificial photosynthetic mimics and potential uses such as optical storage, sensor materials, and self-organizing systems are subjects of growing interest.[51–53] Hydroxyquinolines, which are amphoteric aromatic molecules with two prototropic groups,[38–49] may be good candidates to investigate the catalytic properties and host–guest interactions of zeolites. Because the enolic group and the imino group of 6-hydroxyquinoline (6HQ) are more acidic and more basic, respectively, in the first excited singlet state than in the ground state,[43–45,54] photoexcitation may cause excited-state tautomerization through enol deprotonation to form an anionic intermediate or imine protonation to form a cationic intermediate.

Herein we report the excited-state prototropic equilibrium dynamics of 6HQ encapsulated in Na^+-exchanged faujasite zeolites X (NaX) and Y (NaY).As shown in Figure 2, excited-state proton transfer (ESPT) of 6HQ in zeolitic nanocavities occurs in two steps; the first step is enol deprotonation of the normal species (HOQN, **N**) to form an anionic intermediate species ($^-$OQN, **A**), and the second step is imine protonation of $^-$OQN to form a zwitterionic tautomeric species ($^-$OQNH$^+$, **T**). We neglected the possibility of forming a cationic intermediate in the first ESPT step because the interior of NaX and NaY zeolites is basic

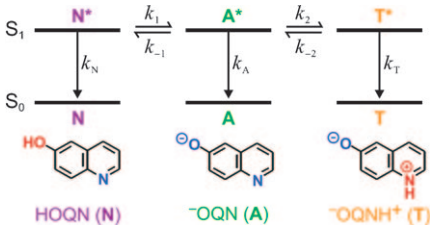

Figure 2. Proton transfer and relaxation of the prototropic species of excited-state 6HQ in microporous catalytic faujasite zeolites.

after being dehydrated at 670 K for 5 h. Thus, as the first step of the ESPT, enol deprotonation of 6HQ induced by proton acceptance of Brønsted base sites in the zeolites occurs predominantly in both NaX and NaY zeolites. Excited-state tautomerization of 6HQ in neutral water is known to take place via an anionic intermediate.[43,45] On the other hand, interesting kinetic features have been observed because geminate recombination, as the reverse reaction of ESPT, also occurs at each step of 6HQ tautomerization due to the confined environment of dehydrated zeolitic nanocavities. In the first step, geminate recombination with rate constant k_{-1} takes place between a proton, which has been transferred from the enolic group of HOQN to a base site in the faujasite zeolite, and $^-$OQN. In the second step, geminate recombination with rate constant of k_{-2} occurs between the imino proton of $^-$OQNH$^+$ and a base site in the zeolite. Consequently, the prototropic equilibria of 6HQ in microporous zeolitic hosts are established in the first excited singlet state.

Results and Discussion

^{129}Xe NMR spectra: Intercalation of 6HQ molecules into zeolitic supercages of NaX and NaY was confirmed by ^{129}Xe NMR spectroscopy (Figure 3). The chemical shift of 6HQ-containing NaY (6HQ-NaY) is 17 ppm larger than that of bare NaY, whereas that of 6HQ-containing NaX (6HQ-NaX) is 10 ppm larger than that of bare NaX. The large chemical shifts of 6HQ-loaded zeolites are attributed to strong interactions with guest 6HQ molecules adsorbed within zeolitic supercages in addition to interactions with supercage walls and other xenon atoms in bare zeolites. A

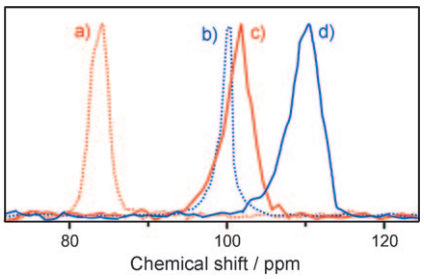

Figure 3. ^{129}Xe NMR spectra of a) bare NaY, b) bare NaX, c) 6HQ-NaY, and d) 6HQ-NaX, showing chemical shifts of $\delta = 84$, 100, 101, and 110 ppm, respectively.

single Lorentzian NMR line is known to reflect the average environment of numerous collisions of xenon atoms on the sweeping timescale of the NMR measurement, although the shift in the NMR line is weighted by collision probabilities.[55,56] The ^{129}Xe NMR spectra of hydroxyquinoline-loaded NaY prepared at low temperature (520 K) were almost the same as the spectrum of bare NaY.[57]

Diffuse-reflectance spectra: The acidity and basicity of faujasite zeolites, which are dependent on the Si/Al ratio, can affect the absorption and emission properties of guest molecules confined in the zeolitic hosts. Consistently, the diffuse-reflectance spectra of 6HQ-NaX and 6HQ-NaY are quite different because of differences in the basicity of two zeolites (Figure 4); NaX (Si/Al 1.4) is more basic than NaY (Si/Al 2.4). Both spectra in Figure 4 indicate that three possible prototropic species of 6HQ exist in the ground state (Figure S1 in the Supporting Information). The absorption spectrum of 6HQ in NaX shows the dominant absorption of HOQN at $\lambda = 325$ nm, with a large shoulder at $\lambda = 365$ nm arising from $^{-}$OQN and additional weak absorption around $\lambda = 430$ nm attributed to $^{-}$OQNH^{+}. Although $^{-}$OQN absorption is much weaker in NaY than in NaX, $^{-}$OQNH^{+} absorption is significantly larger in NaY than in NaX. Thus, the fractions of $^{-}$OQN and $^{-}$OQNH^{+} depend on the Si/Al ratios of faujasite zeolites, which implies that the acid/base sites of zeolites play pivotal roles in controlling the prototropic equilibria of guest molecules. Because NaY is relatively acidic compared with NaX, the fraction of $^{-}$OQNH^{+} formed by protonation of $^{-}$OQN is significantly higher in NaY than in NaX. On the other hand, the absorption of $^{-}$OQNH^{+} around $\lambda = 430$ nm is not observed at any pH of aqueous solutions, although $^{-}$OQN absorption is observed in neutral water as well as in basic aqueous solutions.[43] Considering that tautomeric species are hardly present in aqueous solutions but exist in a significantly high fraction in catalytic zeolites, we can infer that numerous acid and base sites exist together at different locations in a zeolite and that zeolites are more polar than water.

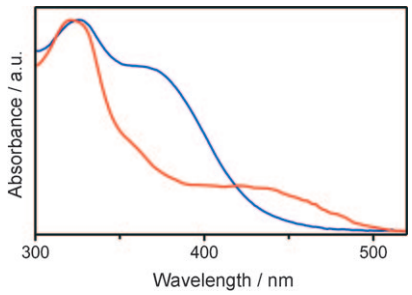

Figure 4. Diffuse-reflectance spectra of 6HQ intercalated in the microporous supercages of NaX (blue line) and NaY (red line).

Emission spectra: The steady-state fluorescence of 6HQ-adsorbed NaX and NaY is mainly emitted from **A*** and **T*** because almost all **N*** molecules undergo deprotonation readily to form **A*** followed by protonation of **A*** to form **T*** in both basic zeolites. On one hand, the emission spectrum of 6HQ-loaded NaX shows **A*** fluorescence predominantly with the emission maximum at $\lambda = 450$ nm and a long red tail around $\lambda = 510$ nm representing formation of **T*** (Figure 5). On the other hand, as $^{-}$OQNH^{+} already exists with a high fraction in NaY at the moment of excitation, the excitation of 6HQ-NaY gives rise to **T*** fluorescence prominently at $\lambda = 513$ nm as well as weak **A*** fluorescence at $\lambda = 450$ nm. The emission spectra of 6HQ in catalytic faujasite zeolites are quite different from those of 6HQ in aqueous solution at any pH (Figure S2 in the Supporting Information); the most noticeable difference is that emission from the excited quinonoid form is not observed in zeolites, although it is observed in aqueous solutions.[43] Zwitterionic **T*** is unstable in aqueous solutions, so that fast charge transfer from the deprotonated enolic ring to the iminium ring of the zwitterionic form occurs rapidly in aqueous solutions to produce a less dipolar quinonoid form as the final product on the first excited singlet potential surface.[43,44]

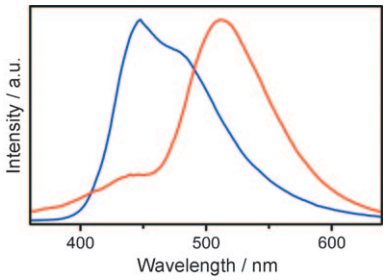

Figure 5. Emission spectra of 6HQ encapsulated in the catalytic nanocavities of NaX (blue line) and NaY (red line) with excitation at $\lambda = 320$ nm.

Time-resolved fluorescence spectra: Figure 6 shows time-resolved fluorescence spectra for various time delays of 6HQ intercalated in NaX and NaY. Although time-dependent

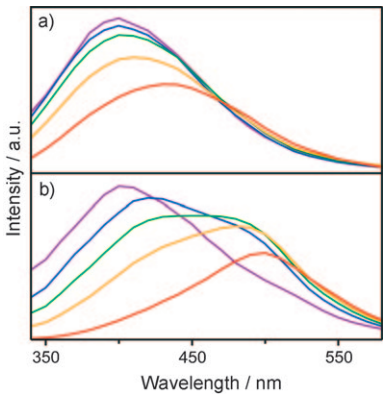

Figure 6. Time-resolved fluorescence spectra of 6HQ encaged in a) NaX and b) NaY after a time delay of 0 (purple), 70 (blue), 200 (green), 500 (yellow), and 2000 ps (red). The samples were excited at $\lambda = 315$ nm.

spectral evolution depends on the zeolite, the fluorescence spectra of both 6HQ-NaX and 6HQ-NaY continuously red-shift with increasing time, that is, a species emitting higher-energy light is transformed into one emitting lower-energy light in the excited state. The time-resolved fluorescence spectra of 6HQ-NaX and 6HQ-NaY at a time delay of 0 ps after excitation have almost the same maximum at $\lambda =$ 404 nm, attributed to **N*** fluorescence. However, those recorded 2000 ps after excitation are quite different from one another; the time-resolved fluorescence spectrum of 6HQ-NaX with the emission maximum at $\lambda = 440$ nm is mainly due to **A*** formed by the enol deprotonation of **N***, whereas that of 6HQ-NaY with the emission maximum at $\lambda = 500$ nm is predominantly due to **T*** generated through imine protonation of **A***. This agrees well with the steady-state fluorescence spectra, which have maxima at $\lambda = 450$ and 513 nm for 6HQ-NaX and 6HQ-NaY, respectively (Figure 5). Imine protonation of **A*** to form **T*** is less favorable in NaX than in NaY because NaX is more basic than NaY. Accordingly, the fraction of **A*** in NaX still remains high even 2000 ps after excitation. The wavelength of the emission maximum of the time-resolved spectrum at 2000 ps is shorter by 13 nm in NaY than that of the steady-state spectrum because the transformation of **A*** into **T*** is not yet complete at that point.

Fluorescence kinetic profiles: Because **N** excitation gives three distinctive fluorescence bands of **N***, **A***, and **T***, the fluorescence kinetic profiles of 6HQ-NaX and 6HQ-NaY with excitation at $\lambda = 315$ nm were monitored at $\lambda = 360$ nm for **N***, at $\lambda = 450$ nm for **A***, and at $\lambda = 600$ nm for **T*** (Figure 7), and kinetic constants were extracted from exponential rise and decay fits (Table 1). The kinetic profile of each prototropic species was monitored without interference of the fluorescence of the other two prototropic species. However, all of the measured kinetic profiles had three components of 36, 210, and 1600 ps regardless of the monitored wavelength, although every profile monitored at $\lambda =$ 450 and 600 nm had an additional fourth component showing very long decay. The initial fractional amplitudes of the three components, which could be negative (indicating rise components) or positive (indicating decay components), varied depending on the monitored wavelength. This implies that the reverse processes of 6HQ tautomerization in faujasite zeolites should be considered as well to fit fluorescence kinetic profiles. The reverse processes make kinetic constants in zeolitic nanocavities more complicated than those in aqueous solutions.[43] Consequently, geminate recombination, as the back-reaction of ESPT, also occurs at each step of 6HQ tautomerization due to the confined and dried environment of faujasite zeolites. The longest decay times observed at $\lambda = 450$ and 600 nm are attributed to the relaxation time constants of **A*** and **T***, respectively, and the rate constant of **N*** relaxation cannot be extracted directly from an experimentally measured kinetic profile because **N*** relaxation is convoluted with ESPT and geminate recombination.

It is worth noting that the three time constants are invariant regardless of whether the zeolite type is NaX or NaYalthough the three initial fractional amplitudes depend on the zeolite type. We attribute these unusual kinetic features to the different numbers of acid and base sites present

Table 1. Fluorescence kinetic constants of 6HQ encapsulated in catalytic faujasite zeolites, taken from Figure 7.

λ_{em} [nm]	Zeolite	Time constants [ps]
360	NaX	36 (0.59)[a] + 210(0.34) + 1600 (0.07)
	NaY	36 (0.35) + 210 (0.56) + 1600 (0.09)
450	NaX	36 (−0.24) + 210 (0.05) + 1600 (0.46) + 9600 (0.49)
	NaY	36 (−0.09) + 210 (0.31) + 1600 (0.53) + 12200 (0.16)
600	NaX	36 (−0.57) + 210 (−0.43) + 1600 (0.07) + 15600 (0.93)
	NaY	36 (−0.80) + 210 (−0.20) + 1600 (0.22) + 18000 (0.78)

[a] Negative and positive values of initial fractional amplitudes indicate rise and decay time constants, respectively.

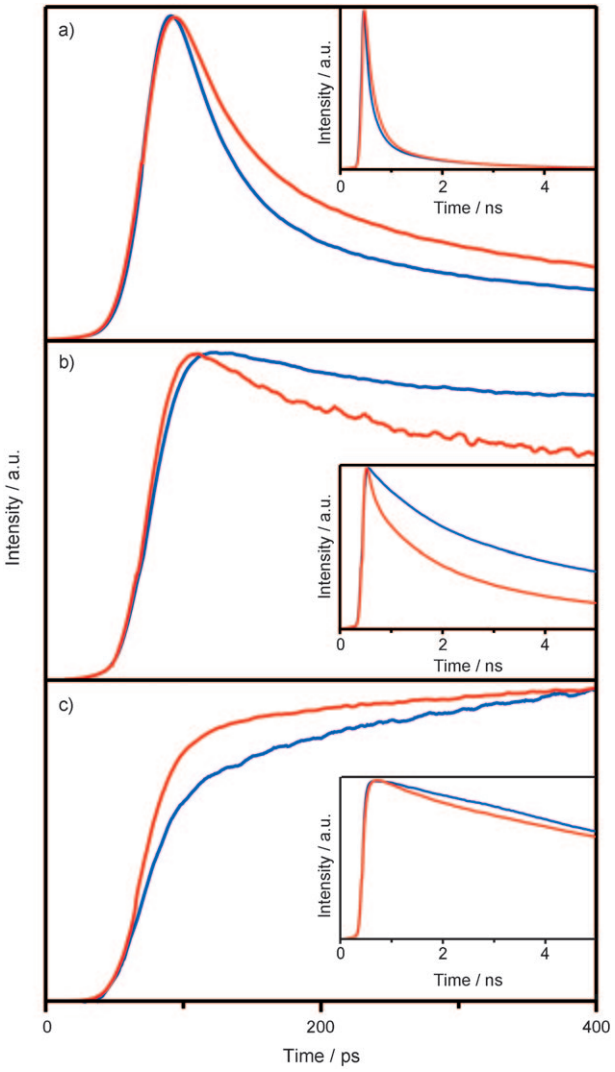

Figure 7. Fluorescence kinetic profiles of 6HQ encapsulated in NaX (blue line) and NaY (red line) excited at $\lambda = 315$ nm and monitored at a) 360 nm, b) 450 nm, and c) 600 nm. Insets display kinetic profiles measured at long time domains to show slow decay kinetics.

in NaX and NaY, which have the same faujasite framework but different Si/Al ratios. Meanwhile, the rate constants of the ESPT of 6HQ in NaX, deduced by computational numerical analysis using the observed time constants and amplitudes given in Table 1 (see below), are different from the respective values in NaY, as shown in Table 2. The proton-transfer and relaxation processes of the prototropic species of excited 6HQ can be depicted as shown in Figure 2, in which k_N, k_A, and k_T denote the radiative and nonradiative relaxation rate constants of **N***, **A***, and **T***, respectively.

Table 2. Excited-state tautomerization and relaxation kinetic constants of 6HQ encaged in zeolites.

Zeolite	k_1^{-1} [ps]	k_{-1}^{-1} [ps]	k_2^{-1} [ps]	k_{-2}^{-1} [ps]	k_N^{-1} [ps]	k_A^{-1} [ps]	k_T^{-1} [ps]
NaX	67	180	420	710	1100	9600	15600
NaY	71	120	380	770	1450	12200	18000

Kinetic analysis: The rate constants of ESPT and **N*** relaxation for 6HQ-NaX and 6HQ-NaY were calculated from computational numerical analyses of the observed kinetic constants given in Table 1. Following the global analysis by Giestas et al.,[58] we conducted numerical analyses of the observed kinetic constants given in Table 1 by using the Mathematica 5.2 program (Wolform Research) to obtain the rate constants of Figure 2. The mechanism of Figure 2 can be translated into Equation (1):

$$\frac{d}{dt}\begin{bmatrix} HOQN \\ {}^{-}OQN \\ {}^{-}OQNH^{+} \end{bmatrix} = \begin{bmatrix} -X & k_{-1} & 0 \\ k_2 & -Y & k_{-2} \\ 0 & k_2 & -Z \end{bmatrix} \times \begin{bmatrix} HOQN \\ {}^{-}OQN \\ {}^{-}OQNH^{+} \end{bmatrix} \quad (1)$$

in which $X=k_1+k_N$, $Y=k_{-1}+k_2+k_A$, and $Z=k_{-2}+k_T$. The observed kinetic constants of $(9600\,ps)^{-1}$ and $(15600\,ps)^{-1}$ were used for k_A and k_T, respectively, of 6HQ-NaX, and $(12200\,ps)^{-1}$ and $(18000\,ps)^{-1}$ were used for k_A and k_T, respectively, of 6HQ-NaY.

The rate constants of excited-state tautomerization and relaxation for 6HQ-NaX and 6HQ-NaY (Table 2) indicate that encapsulation of 6HQ in faujasite zeolitic hosts retards both enol deprotonation of **N*** (k_1) and imine protonation of **A*** (k_2) enormously, compared with the respective values in water.[45] Encapsulation of 6HQ in the dry environment of dehydrated NaY slows down enol deprotonation of **N*** by a factor of 3.4[45] because the enolic group is bound to a weak base site having a limited hydrogen-bond network. Imine protonation of **A*** in NaY is even slower (by a factor of 8.8) than that in water.[45] We consider that the imine protonation of **A*** in a zeolitic nanocavity takes place very slowly because Brønsted acid sites are rare in the framework of faujasite zeolites dried at 670 K. Furthermore, hydrogen bonding required for the protonation of the imino group of **A*** can be made by diffusion of a proton, which is slow in dehydrated zeolites. It is worth noting that both the reverse process of **N*** deprotonation to form **A*** (k_{-1}) and the reverse process of **A*** protonation to form **T*** (k_{-2}) are much faster in faujasite zeolites than in water, although both forward processes are slowed down tremendously in zeolites. We suggest that geminate recombinations occur readily as reverse reactions because the contact ion pairs produced by forward reactions are not well separated in the diffusion-limited environment of dehydrated faujasite zeolites.

The dissimilar Si/Al ratios of NaX and NaY lead to different rate constants of 6HQ-NaX and 6HQ-NaY in excited-state tautomerization. The rate constant of **N*** deprotonation to form **A*** (k_1) is slightly larger in NaX, which has higher basicity, than in NaY, whereas the rate constant of the reprotonation of **A*** to form **N*** (k_{-1}) is much smaller in NaX, which has relatively weak acidity, than in NaY. Furthermore, the rate constant of **A*** protonation to form **T*** (k_2) is smaller in NaX than in NaY, whereas the rate constant of the redeprotonation of **T*** to form **A*** (k_{-2}) is larger in NaX than in NaY. This consequently suggests that the acid/base properties of catalytic faujasite zeolites play an important role in determining both the pathway and the rate constants of acid–base reactions for the guest molecules encaged in zeolitic hosts; protonation processes are facile in NaY having the higher Si/Al ratio, whereas deprotonation processes are easy in NaX with the lower Si/Al ratio. Of note is that all the relaxation processes of **N***, **A***, and **T*** are substantially faster in NaX than in NaY (Table 2), which has the more homogeneous structure due to the larger Si/Al ratio.

Conclusion

Excited-state equilibria involving excited-state proton transfer and geminate recombination of 6HQ encapsulated in catalytic faujasite zeolites NaX and NaY have been explored by measuring steady-state and picosecond time-resolved spectra. The intercalation of 6HQ molecules into zeolitic nanocavities of NaX and NaY has been confirmed by ^{129}Xe NMR spectroscopy. Steady-state spectra indicate that the acid/base properties of zeolites control the absorption and emission properties of 6HQ molecules confined in the zeolitic hosts. The excited-state proton transfer of a 6HQ molecule encapsulated in a zeolitic nanocavity is initiated by deprotonation of the enolic group to form an anionic intermediate and completed by the subsequent protonation of the imino group to form a zwitterionic tautomer. Proton transfer at each tautomerization step of excited-state 6HQ competes with its reverse geminate recombination reaction because of the confined and dry environment of zeolitic supercages. Consequently, excited-state equilibria among three prototropic species of 6HQ are established in microporous catalytic faujasite zeolites. The rate constants of proton transfer of excited 6HQ are determined by the microscopic environment of zeolitic hosts surrounding the guest molecules. Kinetic differences in the two types of faujasite zeolites are attributed to dissimilarities in the acidity/basicity of NaX and NaY.

Experimental Section

Materials: 6HQ (purchased from Sigma-Aldrich) was used after purification by vacuum sublimation. NaX and NaY zeolites were synthesized by following known procedures,[59,60] washed with doubly distilled hot water, and dried in a vacuum oven. After dehydration at 670 K under 10^{-5} torr for 5 h followed by cooling to RT, NaX and NaY zeolites were found to have typical unit cell formulas of $Na_{80}(AlO_2)_{80}(SiO_2)_{112}\cdot 250\,H_2O$ and $Na_{56}(AlO_2)_{56}(SiO_2)_{136}\cdot 250\,H_2O$, respectively. A quartz tube containing a known amount of NaX or NaY and a Pyrex tube containing a known amount of 6HQ to give a desired loading of 0.025 molecules supercage^{-1} were connected to vacuum ports individually, and then maintained at 273 and 670 K, respectively, under vacuum for 2 h. Then the Pyrex tube was joined with the quartz tube at 670 K under vacuum to introduce 6HQ molecules into the supercages of zeolites by subliming 6HQ for 12 h. The quartz tube containing 6HQ-loaded zeolites was sealed off, maintained at 570 K for 3 h, then slowly cooled to RT. A uniform distribution of 6HQ in zeolites was obtained.[61,62] The quartz tube containing the intact sample was directly used for optical measurements, whereas the sample was transferred to a specially designed NMR tube under N_2 atmosphere for ^{129}Xe NMR measurements to confirm that 6HQ molecules were intercalated into the zeolitic hosts. X-ray diffraction was also used to confirm that the zeolitic framework did not change during dehydration and intercalation processes. To obtain the pH-dependent absorption and emission spectra of 6HQ in water, the pH was adjusted by adding dilute aqueous HCl or NaOH to aqueous 6HQ.

Measurements: For the ^{129}Xe NMR studies to obtain information on the distribution of 6HQ into zeolitic supercages, ^{129}Xe gas (Matheson, 99.995 %) was introduced through stopcocks into samples in NMR tubes at RT and allowed to equilibrate to 300 torr. ^{129}Xe NMR spectra were measured by using a Bruker AM 300NMR spectrometer operating at 83 MHz. A homemade spectrometer was used to measure diffuse reflectance. The wavelength of a tungsten/deuterium lamp was selected by using a 0.25 m monochromator (Kratos, GM252) and a sample was mounted at the tangent of an internally MgO coated integrating sphere. The diffuse reflectance of the sample with rejection of specular reflection was detected at right angles to the illuminating beam by using a photomultiplier tube (Hamamatsu, R374). For measurements of emission spectra, the excitation wavelength of a 350 W Xe lamp (Schoeffel, LPS255HR) was selected by using a 0.25 m monochromator (Kratos, GM252), and the emission wavelength by using a 0.25 m monochromator (Kratos, GM252) equipped with a photomultiplier tube (Hamamatsu, R376). Fluorescence kinetic profiles were measured by using a 10 ps streak camera (Hamamatsu, C2830) attached to a CCD detector (Princeton Instruments, RTE-128-H) by exciting samples at $\lambda = 315$ nm with pulses from a Raman shifter, filled with 15 atm CH_4 gas and pumped by the fourth-harmonic pulses of $\lambda = 266$ nm from a 25 ps Nd:YAG laser (Quantel, YG501). Fluorescence wavelengths were selected by using a 0.15 m monochromator (Acton Research, Spectrapro-150). Time-resolved fluorescence spectra were constructed by measuring a fluorescence kinetic profile every 10 nm. Fluorescence kinetic constants were extracted by fitting measured kinetic profiles to computer-simulated kinetic curves convoluted with instrument temporal response functions, and the numerical analyses of the extracted kinetic constants to obtain rate constants were carried out with a computer program (Wolform Research, Mathematica 5.2 for Students). All the measurements were carried out at RT, and all the fluorescence spectra were not corrected for the wavelength-dependent sensitivity variation of detectors.

Acknowledgements

This work was financially supported by research a grant through the National Research Foundation of Korea (NRF) funded by the Ministry of Education, Science, and Technology (2010-0015806). We are also thankful to the SRC program of NRF (2010-0001635) and S.-Y.P. acknowledges the Seoul fellowship and the BK21 scholarship as well.

[1] M. Pauchard, S. Huber, R. Méallet-Renault, H. Maas, R. Pansu, G. Calzaferri, *Angew. Chem.* **2001**, *113*, 2921; *Angew. Chem. Int. Ed.* **2001**, *40*, 2839.
[2] J. K. Thomas, *Chem. Rev.* **2005**, *105*, 1683.
[3] H. García, H. D. Roth, *Chem. Rev.* **2002**, *102*, 3947.
[4] N. J. Turro, *Acc. Chem. Res.* **2000**, *33*, 637.
[5] G. W. Huber, S. Iborra, A. Corma, *Chem. Rev.* **2006**, *106*, 4044.
[6] S. M. Auerbach, K. A. Carrado, P. K. Dutta, *Handbook of Zeolite Science and Technology*, Marcel Dekker, New York, **2003**.
[7] A. Corma, G. W. Huber, L. Sauvanaud, P. O'Connor, *J. Catal.* **2007**, *247*, 307.
[8] V. Ramamurthy, *J. Photochem. Photobiol. C* **2000**, *1*, 145.
[9] M. Pauchard, A. Devaux, G. Calzaferri, *Chem. Eur. J.* **2000**, *6*, 3456.
[10] Y. Xia, B. Gates, Y. Yin, Y. Lu, *Adv. Mater.* **2000**, *12*, 693.
[11] G. Calzaferri, M. Pauchard, H. Maas, S. Huber, A. Khatyr, T. Schaafsma, *J. Mater. Chem.* **2002**, *12*, 1.
[12] B. Muñoz, A. Rámila, J. Pérez-Pariente, I. Díaz, M. Vallet-Regí, *Chem. Mater.* **2003**, *15*, 500.
[13] H. S. Kim, S. M. Lee, K. Ha, C. Jung, Y.-J. Lee, Y. S. Chun, D. Kim, B. K. Rhee, K. B. Yoon, *J. Am. Chem. Soc.* **2004**, *126*, 673.
[14] Y. Kim, A. Das, H. Zhang, P. K. Dutta, *J. Phys. Chem. B* **2005**, *109*, 6929.
[15] M. Castellà-Ventura, Y. Akacem, E. Kassab, *J. Phys. Chem. C* **2008**, *112*, 19045.
[16] F. Trudu, G. Tabacchi, A. Gamba, E. Fois, *J. Phys. Chem. C* **2008**, *112*, 15394.
[17] M. Gil, S. Wang, J. A. Organero, L. Teruel, H. Garcia, A. Douhal, *J. Phys. Chem. C* **2009**, *113*, 11614.
[18] U. Viswanathan, J. T. Fermann, L. K. Toy, S. M. Auerbach, T. Vreven, M. J. Frisch, *J. Phys. Chem. C* **2007**, *111*, 18341.
[19] S. Li, A. Zheng, Y. Su, H. Zhang, L. Chen, J. Yang, C. Ye, F. Deng, *J. Am. Chem. Soc.* **2007**, *129*, 11161.
[20] L. Peng, P. J. Chupas, C. P. Grey, *J. Am. Chem. Soc.* **2004**, *126*, 12254.
[21] J.-P. Joly, A. Perrard, *Langmuir* **2001**, *17*, 1538.
[22] C. Lee, D. J. Parrillo, R. J. Gorte, W. E. Farneth, *J. Am. Chem. Soc.* **1996**, *118*, 3262.
[23] B. Onida, F. Geobaldo, F. Testa, R. Aiello, E. Garrone, *J. Phys. Chem. B* **2002**, *106*, 1684.
[24] M. Sierka, J. Sauer, *J. Phys. Chem. B* **2001**, *105*, 1603.
[25] Y.-S. Lee, H. Yu, O.-H. Kwon, D.-J. Jang, *Phys. Chem. Chem. Phys.* **2008**, *10*, 153.
[26] R. A. van Santen, G. J. Kramer, *Chem. Rev.* **1995**, *95*, 637.
[27] A. Corma, *Chem. Rev.* **1995**, *95*, 559.
[28] O.-H. Kwon, H. Yoo, D.-J. Jang, *Eur. Phys. J. D* **2002**, *18*, 69.
[29] L. Benco, Th. Demuth, J. Hafner, F. Hutschka, *Chem. Phys. Lett.* **2000**, *324*, 373.
[30] D. Barthomeuf, *J. Phys. Chem.* **1984**, *88*, 42.
[31] M. Müller, G. Harvey, R. Prins, *Microporous Mesoporous Mater.* **2000**, *34*, 281.
[32] S.-Y. Park, O.-H. Kwon, T. G. Kim, D.-J. Jang, *J. Phys. Chem. C* **2009**, *113*, 16110.
[33] M. E. Tuckerman, D. Marx, M. Parrinello, *Nature* **2002**, *417*, 925.
[34] O. F. Mohammed, D. Pines, E. T. J. Nibbering, E. Pines, *Angew. Chem.* **2007**, *119*, 1480; *Angew. Chem. Int. Ed.* **2007**, *46*, 1458.
[35] R. M. Tolbert, K. M. Solntsev, *Acc. Chem. Res.* **2002**, *35*, 19.
[36] K. M. Solntsev, C. E. Clower, L. M. Tolbert, D. Huppert, *J. Am. Chem. Soc.* **2005**, *127*, 8534.
[37] R. Gepshtein, P. Leiderman, L. Genosar, D. Huppert, *J. Phys. Chem. A* **2005**, *109*, 9674.
[38] S.-Y. Park, O.-H. Kwon, Y.-S. Lee, D.-J. Jang, *J. Phys. Chem. A* **2009**, *113*, 10589.
[39] S.-Y. Park, Y.-S. Lee, O.-H. Kwon, D.-J. Jang, *Chem. Commun.* **2009**, 926.
[40] S.-Y. Park, B. Kim, Y.-S. Lee, O.-H. Kwon, D.-J. Jang, *Photochem. Photobiol. Sci.* **2009**, *8*, 1611.
[41] S.-Y. Park, D.-J. Jang, *J. Am. Chem. Soc.* **2010**, *132*, 297.

[42] O.-H. Kwon, Y.-S. Lee, B. K. Yoo, D.-J. Jang, *Angew. Chem.* **2006**, *118*, 429; *Angew. Chem. Int. Ed.* **2006**, *45*, 415.
[43] T. G. Kim, Y. Kim, D.-J. Jang, *J. Phys. Chem. A* **2001**, *105*, 4328.
[44] T. G. Kim, M. R. Topp, *J. Phys. Chem. A* **2004**, *108*, 10060.
[45] Y.-S. Lee, O.-H. Kwon, H. J. Park, J. Franz, D.-J. Jang, *J. Photochem. Photobiol. A* **2008**, *194*, 105.
[46] H. J. Park, O.-H. Kwon, C. S. Ah, D.-J. Jang, *J. Phys. Chem. B* **2005**, *109*, 3938.
[47] O.-H. Kwon, T. G. Kim, Y.-S. Lee, D.-J. Jang, *J. Phys. Chem. B* **2006**, *110*, 11997.
[48] S.-Y. Park, Y.-S. Lee, D.-J. Jang, *Phys. Chem. Chem. Phys.* **2008**, *10*, 6703.
[49] O.-H. Kwon, H. Doo, Y.-S. Lee, D.-J. Jang, *ChemPhysChem* **2003**, *4*, 1079.
[50] O.-H. Kwon, H. Yu, D.-J. Jang, *J. Phys. Chem. B* **2004**, *108*, 3970.
[51] J. W. Lee, S. Samal, N. Selvapalam, H.-J. Kim, K. Kim, *Acc. Chem. Res.* **2003**, *36*, 621.
[52] J. Mohanty, W. M. Nau, *Angew. Chem.* **2005**, *117*, 3816; *Angew. Chem. Int. Ed.* **2005**, *44*, 3750.
[53] C. Raja, K. Ananthanarayanan, P. Natarajan, *Eur. Polym. J.* **2006**, *42*, 495.
[54] J. L. Pérez-Lustres, F. Rodriguez-Prieto, M. Mosquera, T. A. Senyushkina, N. P. Ernsting, S. A. Kovalenko, *J. Am. Chem. Soc.* **2007**, *129*, 5408.
[55] R. Ryoo, S.-B. Liu, L. C. de Menorval, K. Takegoshi, B. Chmelka, M. Trecoske, A. Pines, *J. Phys. Chem.* **1987**, *91*, 6575.
[56] M.-A. Springuel-Huet, J.-L. Bonardet, A. Gédéon, J. Fraissard, *Magn. Reson. Chem.* **1999**, *37*, S1.
[57] W.-K. Kang, S.-J. Cho, M. Lee, D.-H. Kim, R. Ryoo, K.-H. Jung, D.-J. Jang, *Bull. Korean Chem. Soc.* **1992**, *13*, 140.
[58] L. Giestas, C. Yihwa, J. C. Lima, C. Vautier-Giongo, A. Lopes, A. L. Maçanita, F. H. Quina, *J. Phys. Chem. A* **2003**, *107*, 3263.
[59] M. Miyake, M. Yoshino, M. Matsuda, M. Kiguchi, Y. Taniguchi, H. Uehara, M. Sato, *J. Mater. Sci.* **1999**, *34*, 5509.
[60] U. Vietze, O. Krauß, F. Laeri, G. Ihlein, F. Schuth, B. Limburg, M. Abraham, *Phys. Rev. Lett.* **1998**, *81*, 4628.
[61] R. Hoppe, G. Schulz-Ekloff, D. Wöhrle, C. Kirschhock, H. Fuess, *Langmuir* **1994**, *10*, 1517.
[62] A. N. Fitch, H. Jobic, A. Renouprez, *J. Phys. Chem.* **1986**, *90*, 1311.

Received: March 24, 2010
Published online: September 17, 2010

